Eur. Phys. J. D (2016) 70: 268
DOI: 10.1140/epjd/e2016-70516-7

THE EUROPEAN PHYSICAL JOURNAL D

Regular Article

Interference effects on (e, 2e) electron momentum profiles: a comparative study for CCl_4 and CF_4*

Noboru Watanabe, Keisuke Katafuchi, Masakazu Yamazaki, and Masahiko Takahashi[a]

Institute of Multidisciplinary Research for Advanced Materials, Tohoku University, 980-8577 Sendai, Japan

Received 17 August 2016 / Received in final form 30 September 2016
Published online 22 December 2016 –

Abstract. Interference effects on electron momentum density distributions have been studied using electron momentum spectroscopy (EMS) for the three outermost orbitals of CCl_4, which are constructed from the Cl 3p nonbonding atomic orbitals. The EMS experiment was conducted in the symmetric noncoplanar geometry at an incident electron energy of 2.0 keV. Interference pattern has then been obtained by dividing the experimental data by distorted-wave-Born-approximation cross section for an isolated Cl 3p atomic orbital. A comparison with the result of our earlier study on CF_4 [N. Watanabe, X.-J. Chen, M. Takahashi, Phys. Rev. Lett. **108**, 173201 (2012)] has demonstrated that the period of the interference pattern reflects the internuclear distance between the constituent halogen atoms. Furthermore, the present result strongly suggests that distorted-wave effects lead to partial destruction of the interference for CCl_4 at large momentum.

1 Introduction

Electron momentum spectroscopy (EMS), also known as binary (e, 2e) spectroscopy, is now a well-established technique for the investigation of the electronic structures of atoms and molecules [1–7]. The basis of the technique is the observation of electron impact ionization reactions under the high-energy Bethe-ridge conditions. In the kinematical conditions, the triple-differential cross section of electron impact ionization (the EMS cross section) is directly related to the one-electron momentum density distribution of the ionized orbital. EMS thus offers an opportunity to study various properties of molecular orbitals (MOs) in momentum-space (p-space) [8,9], rather than through the commonly used position-space (r-space) representation.

One of the notable features of a p-space wave function $\psi(\boldsymbol{p})$ is that for molecules, the information about the equilibrium nuclear positions $\boldsymbol{R}_j$ appears only in phase factors, $\exp(i\boldsymbol{p}\cdot\boldsymbol{R}_j)$, introduced by the Dirac-Fourier transform. Hence, the electron momentum distribution of a MO, $|\psi(\boldsymbol{p})|^2$, inherently possesses cosinusoidal modulations, for instance, that with periodicity of $2\pi/R_{jk}$ along the direction of the line connecting the jth and kth constituent atoms, separated by the distance R_{jk} [3–6]. The interference phenomena of this kind are called bond oscillation [10,11].

Although bond oscillation is a fundamental property of electron momentum distributions [8,9], the first experimental evidence of its presence was not given by EMS until 2012; a joint study of the Sendai (e, 2e) group and the Hefei (e, 2e) group on CF_4 represented the first time that EMS cross sections were analyzed in depth to make bond oscillation visible [12]. The study also showed the sensitivity of bond oscillation to the spatial orientation of the constituent AOs. Later, the Hefei group performed a high energy-resolution EMS study on H_2 [13], in which the observed deviation from the Franck-Condon principle in vibrational ratio was attributed to interference effects. We the Sendai group also conducted an EMS study on the same molecule, paying special attention to observing a full period of the interference pattern [14]. More recently, the Hefei group and the Sendai group independently reported the experimental observation of bond oscillation for a more complicated compound, SF_6 [15,16]. A detailed analysis of the results by the Sendai group [16] has shown that the interference pattern provides a wealth of information about the spatial distribution and symmetry of the MO in interest.

In the present study we extend our earlier work on the bond oscillation of CF_4 to that of CCl_4 to get further insights into the interference phenomena. CCl_4 and CF_4 are both tetrahedral molecules and their valence electronic structures closely resemble each other. Indeed, the three outermost MOs of CCl_4 and CF_4 are constructed from the Cl 3p and F 2p AOs, respectively. In contrast to the resemblance of the valence electronic structure, the Cl-Cl internuclear distance of CCl_4 is much longer than the F-F distance of CF_4, and thus a comparative

* Contribution to the Topical Issue "Many Particle Spectroscopy of Atoms, Molecules, Clusters and Surfaces", edited by A.N. Grum-Grzhimailo, E.V. Gryzlova, Yu.V. Popov, and A.V. Solov'yov.

[a] e-mail: masahiko@tagen.tohoku.ac.jp

study for these molecules provides an ideal opportunity to examine how the internuclear distance affects the interference pattern. For this purpose, an EMS experiment on CCl_4 has been carried out by using one of our highly sensitive EMS spectrometers [17]. Considerable improvement in the statistical accuracy of data has been achieved as compared with that of the EMS study on CCl_4 reported in the literature [18]. Comparison between the interference patterns of CCl_4 and CF_4 has demonstrated that their periods sensitively reflect the internuclear distances. Furthermore, it has been found that for CCl_4, distorted-wave effects [4,6] considerably affect the interference pattern at large momentum.

2 Experiment

EMS is a high-energy electron-impact ionization experiment that involves coincident detection of the inelastically scattered and ejected electrons [1–7]. The binding energy, $E_{\rm bind}$, and the momentum of the target electron before ionization, $\boldsymbol{p}$, can be determined by means of the following energy and momentum conservation laws:

$$E_{\rm bind} = E_0 - E_1 - E_2, \tag{1}$$

$$\boldsymbol{p} = \boldsymbol{p}_1 + \boldsymbol{p}_2 - \boldsymbol{p}_0. \tag{2}$$

Here E_j's and $\boldsymbol{p}_j$'s ($j = 0, 1, 2$) are the energies and momenta of the incident, inelastically scattered, and ejected electrons, respectively.

An EMS experiment on CCl_4 was conducted at $E_0 = 2.0$ keV in the symmetric noncoplanar geometry, where the two outgoing electrons having equal energies and making equal polar angles of 45° with respect to the incident electron beam axis are detected. In this scattering kinematics, the magnitude of the target electron momentum, $p = |\boldsymbol{p}|$, can be determined from the out-of-plane azimuthal angle difference between the two outgoing electrons ($\Delta\phi = \phi_2 - \phi_1 - \pi$). Details of the spectrometer used have been given elsewhere [17]. Briefly, it consists of an electron gun, a sample inlet systems with eight gas nozzles, decelerating electrostatic lenses, a spherical analyzer, and a pair of position-sensitive detectors. Since a spherical analyzer maintains the azimuthal angles of the electrons, both the energies and angles can be determined from their arrival positions at the detectors.

Experimental results for CCl_4 were obtained by accumulating data at an ambient sample gas pressure of 2.9×10^{-4} Pa for four weeks runtime. Commercially available CCl_4 liquid (Kanto Chemicals, >99.9%) was subjected to repeated freeze-pump-thaw cycles before use. During the measurement the electron gun produced an electron beam of typically 42 μA in the interaction region. In order to achieve higher energy resolution, two outgoing electrons were decelerated to 2.5:1 using an electrostatic lens system prior to energy analysis. The resulting instrumental energy- and momentum-resolution employed was 2.5 eV full width at half maximum (FWHM) and about 0.20 a.u. at $p = 1$ a.u., respectively. No detectable impurities were observed in the binding energy spectra.

3 Theory

3.1 Theoretical momentum profiles

Within the plane wave impulse approximation (PWIA), the EMS cross section is given by:

$$\sigma_{\rm EMS}(p) = (2\pi)^4 \frac{p_1 p_2}{p_0} f_{\rm ee} M(p). \tag{3}$$

Here $f_{\rm ee}$ is the electron-electron collision factor and $M(p)$ is the quantity called momentum profile [4], which is expressed as follows [3–7]:

$$M(p) = \frac{1}{4\pi} S_\alpha d_\alpha \int |\psi_\alpha(\boldsymbol{p})|^2 \, d\Omega_{\boldsymbol{p}}, \tag{4}$$

where $\psi_\alpha(\boldsymbol{p})$ is the p-space representation of the normalized Dyson orbital for the molecule and S_α is the spectroscopic factor. $(4\pi)^{-1} \int d\Omega_{\boldsymbol{p}}$ represents the spherical averaging due to the random orientation of gaseous molecular targets and d_α denotes the degeneracy of the orbital. The momentum profile therefore corresponds to the spherically-averaged electron momentum density distribution of the ionized orbital.

For comparison with experiment, we calculated theoretical momentum profiles of CCl_4 using the target Kohn-Sham (KS) approximation [19]. Briefly, the KS orbitals of the molecule were obtained by means of density functional theory (DFT) along with the Becke-3-parameters-Lee-Yang-Parr (B3LYP) functional [20] and aug-cc-pVTZ basis [21], and they were used as normalized Dyson orbitals. The DFT calculations were performed using the Gaussian03 program [22]. The KS orbitals were subsequently converted to $M(p)$'s with the aid of HEMS program developed by Bawagan et al. [23]. The theoretical momentum profiles thus obtained were then folded with the instrumental momentum resolution according to the procedure of Migdall et al. [24] for comparison with experiment.

3.2 Interference factor

In analysis of bond oscillation we have used the following model, which was originally developed to examine interference patterns in CF_4 [12]. The model has been described in detail elsewhere [16]. Briefly, the three outermost MOs of CCl_4 are approximately described by equation (5), since they consist of the Cl 3p AOs,

$$\psi_\alpha(\boldsymbol{r}) = \sum_{j=1}^{4} c_j \chi_{3\rm p}(r_j) \left[\sum_{m=-1}^{1} a_{j,m} Y_{1,m}(\hat{\boldsymbol{r}}_j) \right]. \tag{5}$$

Here c_j's are coefficients of the linear combination of AOs expansion, $\chi_{3\rm p}(r_j)$ is the radial part of the Cl 3p AO centered at the jth Cl atom position $\boldsymbol{R}_j$, and $\boldsymbol{r}_j = \boldsymbol{r} - \boldsymbol{R}_j$. $Y_{1,m}$ denotes spherical harmonics with the total angular momentum quantum number of $\ell = 1$ and magnetic quantum number of m. Spatial orientation of the jth 3p AO

is defined by a set of coefficients $a_{j,m}$'s, which satisfy $|a_{j,-1}|^2 + |a_{j,0}|^2 + |a_{j,1}|^2 = 1$. Here $a_{j,m}$'s are taken so that the values of c_j's become positive.

Taking the Dirac-Fourier transform of equation (5) the p-space representation of the molecular orbital is obtained as follows:

$$\psi_\alpha(\boldsymbol{p}) = \chi_{3\mathrm{p}}(p) \sum_{j=1}^{4} c_j \exp(i\boldsymbol{p}\cdot\boldsymbol{R}_j) \sum_{m=-1}^{1} a_{j,m} Y_{1,m}(\hat{\boldsymbol{p}}), \tag{6}$$

with

$$\chi_{3\mathrm{p}}(p) = i\sqrt{\frac{2}{\pi}} \int j_1(pr)\, \chi_{3\mathrm{p}}(r)\, r^2 dr. \tag{7}$$

Here $j_1(pr)$ is the spherical Bessel function of order 1. From equations (3), (4), and (6), it follows that

$$\sigma_{\mathrm{EMS}}(p) = \sigma_{3\mathrm{p}}(p)\, S_\alpha d_\alpha \sum_{j,k} c_j c_k \int \exp(i\boldsymbol{p}\cdot\boldsymbol{R}_{jk}) \times \left[\sum_{m,m'} a_{j,m} a^*_{k,m'} Y_{1,m}(\hat{\boldsymbol{p}})\, Y^*_{1,m'}(\hat{\boldsymbol{p}})\right] d\Omega_{\boldsymbol{p}}, \tag{8}$$

where $\boldsymbol{R}_{jk} = \boldsymbol{R}_j - \boldsymbol{R}_k$ and $\sigma_{3\mathrm{p}}(p) = 4\pi^3(p_1 p_2/p_0) f_{\mathrm{ee}} |\chi_{3\mathrm{p}}(p)|^2$, which corresponds to the EMS cross section for the 3p AO of an isolated Cl atom. After expanding the exponential, $\exp(i\boldsymbol{p}\cdot\boldsymbol{R}_{jk})$, in terms of spherical harmonics, the integration over $\Omega_{\boldsymbol{p}}$ is performed. Then it is shown that the EMS cross section can be written as:

$$\sigma_{\mathrm{EMS}}(p) = \sigma_{3\mathrm{p}}(p)\, S_\alpha I_\alpha(p), \tag{9}$$

with

$$I_\alpha(p) = d_\alpha h_\alpha \left[1 + \sum_{j\neq k} \left\{C^{(0)}_{jk}\, j_0(pR_{jk}) + C^{(2)}_{jk}\, j_2(pR_{jk})\right\}\right]. \tag{10}$$

Here $h_\alpha = \Sigma_j c_j^2$ and $R_{jk} = |\boldsymbol{R}_{jk}|$. The coefficients of the spherical Bessel functions of order 0 and 2 are given by:

$$C^{(0)}_{jk} = c_j c_k \cos\theta_{jk} \Big/ \sum_j c_j^2, \tag{11}$$

$$C^{(2)}_{jk} = c_j c_k \left[\cos\theta_{jk} - 3\left(\hat{\boldsymbol{u}}_j\cdot\hat{\boldsymbol{R}}_{jk}\right)\left(\hat{\boldsymbol{u}}_k\cdot\hat{\boldsymbol{R}}_{jk}\right)\right] \Big/ \sum_j c_j^2, \tag{12}$$

with $\hat{\boldsymbol{R}}_{jk} = \boldsymbol{R}_{jk}/|\boldsymbol{R}_{jk}|$. Here θ_{jk} is the angle between the orientations of the constituent 3p AOs located on the jth and kth Cl atoms. $\hat{\boldsymbol{u}}_j$ and $\hat{\boldsymbol{u}}_k$ are unit vectors codirectional with the orientations of the 3p AOs.

CCl_4 has only one Cl-Cl distance, R_{ClCl}, and hence, the function $I_\alpha(p)$ can be simplified to

$$I_\alpha(p) = d_\alpha h_\alpha \left[1 + C_0 j_0(pR_{\mathrm{ClCl}}) + C_2 j_2(pR_{\mathrm{ClCl}})\right], \tag{13}$$

where $C_0 = \Sigma C^{(0)}_{jk}$ and $C_2 = \Sigma C^{(2)}_{jk}$. Since $I_\alpha(p)$ governs the oscillatory feature of the interference pattern, it is henceforth referred to as the interference factor.

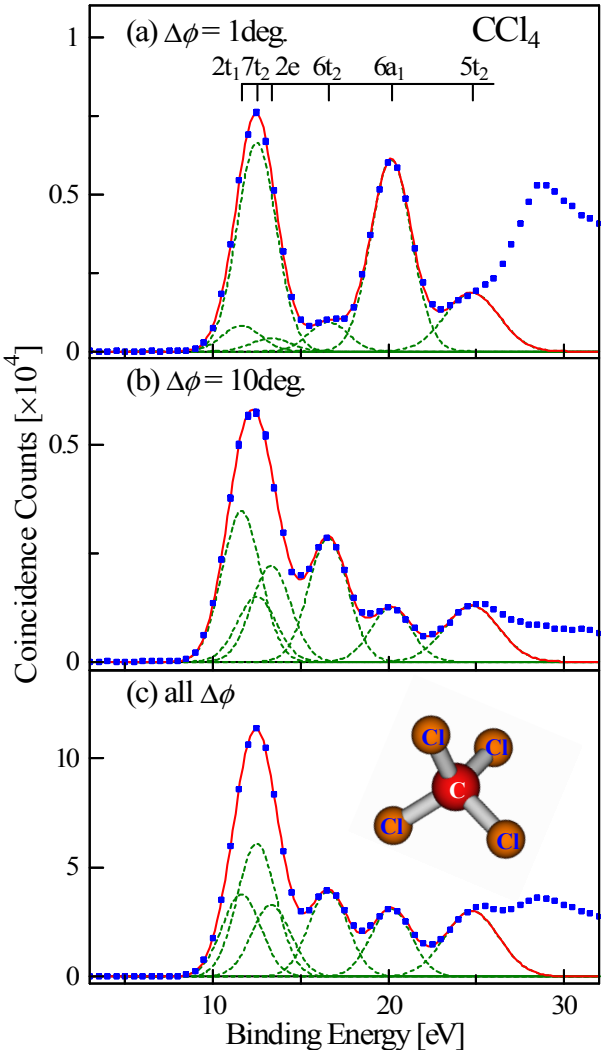

Fig. 1. Binding energy spectra of CCl_4. Vertical bars indicate the ionization energies of the outer valence orbitals. The broken curves represent the Gaussian deconvolution functions of the data and the solid curve their sum.

4 Results and discussion

4.1 Binding energy spectra

CCl_4 belongs to the T_d point group and its electronic configuration can be written as:

$$(\mathrm{core})^{42}(5a_1)^2(5t_2)^6(6a_1)^2(6t_2)^6(2e)^4(7t_2)^6(2t_1)^6.$$

Figure 1 shows examples of experimental binding energy spectra of CCl_4. To illustrate the momentum dependent variations of the band intensities, the spectra at two specific azimuthal angle differences, $\Delta\phi = 1°$ and $10°$, are depicted in the figure, together with the $\Delta\phi$-angle integrated spectrum. Vertical bars indicate the ionization energies reported in references [25,26].

To extract the contributions from individual ionization bands, a deconvolution procedure was used. In the procedure a Gaussian curve was assumed for each ionization

band. The energy-position and width of each Gaussian curve were determined by taking into account the instrumental energy resolution together with Franck-Condon widths estimated from photoelectron spectroscopy studies [25,26]. In Figure 1 the deconvoluted curves are shown as dashed curves and their sum as a solid curve. A similar fitting procedure was applied to a series of binding energy spectra at each $\Delta\phi$. Then experimental momentum profile of each ionization band was produced by plotting the area under the corresponding Gaussian curve as a function of p. It should be noted that since the binding energies of the three outermost orbitals are 11.7, 12.4, and 13.4 eV [25], respectively, their ionization bands are inextricably overlapped due to rather poor energy-resolution (2.5 eV FWHM) employed. This is partly because the present measurement aimed to achieve high statistical accuracy at the expense of energy resolution in order to obtain the interference pattern over wide p region. Hence, for these orbitals, the sum of their contributions $(2t_1{+}7t_2+2e)$, is considered here.

4.2 Momentum profiles

The experimental momentum profiles of the $(2t_1{+}7t_2{+}2e)$, $6t_2$, and $6a_1$ orbitals are shown in Figures 2a–2c, together with the associated PWIA calculations. Inserted in the figure are theoretical electron density distributions of the molecular orbitals in r-space. For making a comparison with theory, the $(2t_1{+}7t_2{+}2e)$ experimental momentum profile has been height-normalized to the corresponding calculation at $p = 0.63$ a.u. The scaling factor thus obtained has subsequently been applied to the individual experimental results so that all the experimental momentum profiles share a common intensity scale. It should be noted that for the $6a_1$ theoretical momentum profile, an additional factor (0.87) has to be multiplied to reproduce the experimental result. This implies that the spectroscopic factor of the $6a_1^{-1}$ band is about 0.87 times smaller than those of the four highest ionization bands. It is reasonably consistent with the results of the ADC(3) calculation reported by Grisogono et al. [18]. The theoretical calculation has predicted that the sum of the spectroscopic factors of the $6a_1^{-1}$ manifolds at $E_{\rm bind}$ ∼20.6 eV is 0.75, while the values of S_α for the $2t_1^{-1}$, $7t_2^{-1}$, $2e^{-1}$, and $6t_2^{-1}$ ionization are 0.91, 0.91, 0.90, and 0.87, respectively.

A comparison between experiment and theory shows that all in all, the PWIA calculation qualitatively reproduces the experimental momentum profiles. In particular, the theoretical predictions for the $6t_2$ and $6a_1$ orbitals have satisfactorily reproduced the experiment at $p >\sim 1.6$ a.u. A close look at Figures 2a–2c, however, indicates that the overall agreement with theory is not quantitative. The theoretical calculation noticeably underestimates the intensity at $p >\sim 1.6$ a.u. for all three momentum profiles. Furthermore, the $(2t_1{+}7t_2+2e)$ experimental result exhibits larger intensity than the theoretical prediction at small p. Similar tendencies have also been observed by Grisogono et al. [18], but higher statistical accuracy achieved in the present study allows us to make a more detailed comparison of experiment with theory.

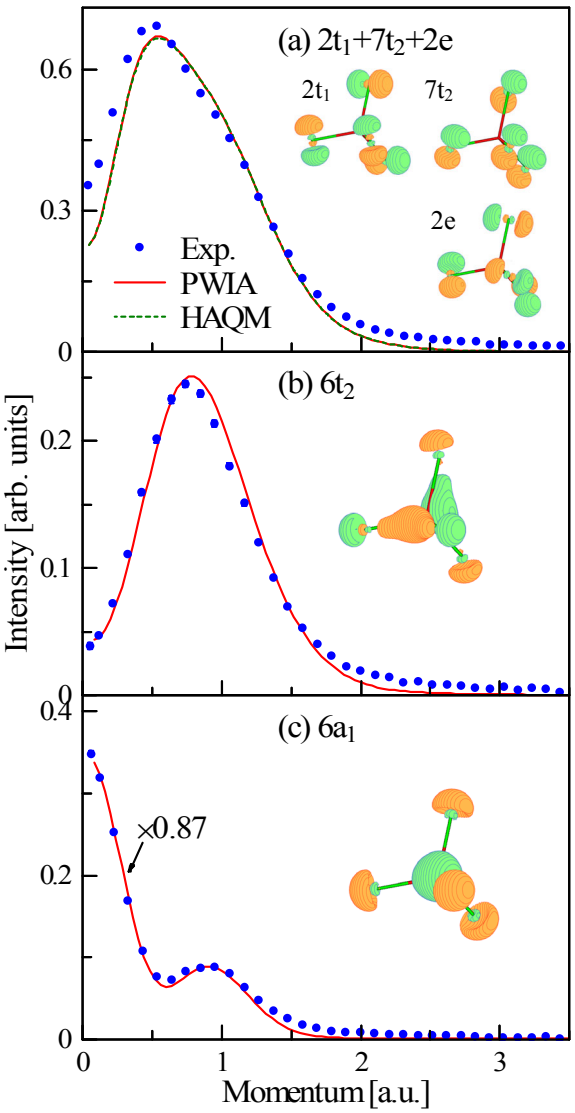

Fig. 2. Comparison between experimental and theoretical momentum profiles for the (a) $(2t_1{+}7t_2{+}2e)$, (b) $6t_2$, and (c) $6a_1$ orbitals of CCl_4. The solid lines represent the PWIA calculation. The inserted figures are the corresponding theoretical electron density distributions in r-space.

The intensity differences observed at $p >\sim 1.6$ a.u. can be attributed to the influence of the distortion of the incoming and outgoing electron waves which participate in the electron-impact ionization process [4,6]. Since p-space wave functions are related to r-space wave functions by the Dirac-Fourier transform, the larger p component of a momentum profile involves contributions from the smaller r region, near the nucleuses, where the influences of the target potential to the electron waves should be sizable. Distorted-wave effect is therefore pronounced for the large p components of momentum profiles [4,6,27,28], and the effect lead to higher intensity than the PWIA calculation at large p.

For the small p region of the $(2t_1{+}7t_2{+}2e)$ momentum profile, however, the observed discrepancy between experiment and theory may possibly stem not only from distorted-wave effects, but also from the influence of molecular vibration. This is because recent EMS studies have shown that molecular vibration may considerably affect momentum profiles of polyatomic molecules at small p [29–34]. We thus performed an additional theoretical calculation for the $(2t_1{+}7t_2{+}2e)$ orbitals, which takes vibrational effects into account using the harmonic analytical quantum mechanical (HAQM) method [29,33]. The computed result is shown by the chain line in Figure 2a. It is immediately clear from the figure that taking into account vibrational effects causes no appreciable change of the momentum profile, indicating that one can safely neglect the influence of nuclear dynamics in analyzing the experimental data on the nonbonding orbitals. A plausible explanation of the difference between experiment and theory is distorted-wave effect again. Our earlier EMS study on Ne has shown that taking into account the effect leads to the slight increase in relative intensity of the small p component of the 2p momentum profile [28]. It is likely that such an influence appears also for the nonbonding orbitals consisting of p-type AOs, and thus the distorted-wave effect is considered in the data analysis for extracting the interference pattern from the $(2t_1{+}7t_2 + 2e)$ momentum profile, as discussed below.

4.3 Bond oscillation

Within the model described in Section 3.2, the momentum profiles of the Cl 3p nonbonding orbitals are expressed as a product of interference factor, $I_\alpha(p)$, and the EMS cross section of the 3p AO, $\sigma_{3p}(p)$. It is thus expected that interference factor can be obtained by dividing the $(2t_1{+}7t_2 + 2e)$ experimental momentum profile by $\sigma_{3p}(p)$. Here, to take into account distorted-wave effect, $\sigma_{3p}(p)$ was calculated with the distorted-wave Born approximation (DWBA) [35] using the Hartree-Fock (HF) wave function reported by Clementi and Roetti [36]. Figure 3a shows the experimental interference factor obtained for the $(2t_1{+}7t_2{+}2e)$ orbitals. The theoretical calculation is also presented in the figure in the form of the interference factor, which was generated by dividing the PWIA momentum profile by the Cl 3p PWIA cross section. Owing to the presence of a node at $p \sim$3.3 a.u. in the p-space Cl 3p AO, the PWIA curve shows a sudden change of intensity at large p, which is not taken into account in the following discussion. It is evident from Figure 3a that the experimental result exhibits oscillation, as expected, and this observation is supported by the PWIA calculation.

In our earlier study on CF_4 [12], bond oscillation has been investigated for the $1t_1$, $4t_2$, and $1e$ orbitals of the molecule, all of which consist of F 2p AOs. For comparison, the associated interference factor is presented in Figure 3b, which was obtained by dividing the $(1t_1{+}4t_2 + 1e)$ experimental momentum profile measured at $E_0 = 2.0$ keV by the F 2p DWBA cross section, $\sigma_{2p}(p)$. Also depicted in the figure is the corresponding PWIA calculation. Comparison of Figures 3a and 3b shows that the interference patterns of these molecules resemble each other, while the positions of the maxima and minima for CCl_4 are shifted to lower p compared to those for CF_4, except for the maxima at $p \sim 0$.

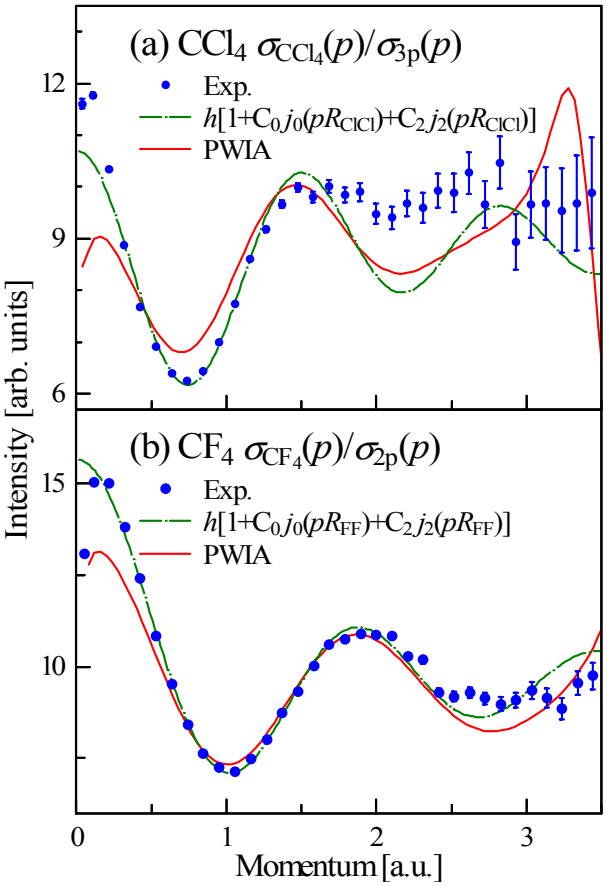

Fig. 3. Comparison of experimental and theoretical interference patterns for the (a) $(2t_1{+}7t_2{+}2e)$ orbitals of CCl_4 and (b) $(1t_1{+}4t_2{+}1e)$ orbitals of CF_4. The solid lines represent the PWIA calculation, and chain lines are fitting curves, which are employed to reproduce the experimental results with h, C_0, C_2, and R_{ClCl} or R_{FF} being used as fitting parameters.

The clue for understanding the observations lies in the analytical interference factor, $I_\alpha(p)$. As can be seen from equations (11) and (12), the values of the coefficients involved in the interference factor, $C_{jk}^{(0)}$ and $C_{jk}^{(2)}$, are determined only by the spatial orientation of the constituent AOs. The directions of the Cl 3p AOs in the $2t_1$, $7t_2$, and $2e$ MOs are the same as those of the F 2p AOs in the $1t_1$, $4t_2$, and $1e$ MOs, respectively, and $I_\alpha(p)$'s of CCl_4 and CF_4 have a common functional form. Hence, the interference patterns of these molecules should exhibit similar oscillatory structures, while their periods are different from one another due to the internuclear distance involved in the argument of the spherical Bessel functions. Reflecting the Cl-Cl distance being longer than the F-F distance, the oscillation of CCl_4 has a shorter period. The above discussion provides a rational account of the observed oscillatory

features, and the results demonstrate that bond oscillation certainly brings information of the molecular geometry.

For a quantitative analysis, the function $h[1 + C_0 j_0(pR_{ClCl}) + C_2 j_2(pR_{ClCl})]$ has subsequently been employed as a fitting curve to reproduce the experiment with R_{ClCl}, h, C_0, and C_2 being used as fitting parameters. The best fit to experiment is presented as a chain line. The resulting R_{ClCl} value of 4.91 Bohr is found to be in reasonable agreement with 5.46 Bohr reported by electron diffraction [37]. In our earlier study, a similar attempt was made for CF_4. The F-F distance determined from the fitting procedure was $R_{FF} = 4.02$ Bohr, showing excellent agreement with 4.07 Bohr reported in reference [38]. One may notice that the deviation of the obtained value from reliable internuclear distance is considerably larger for CCl_4. This is mainly due to the influence of the instrumental momentum resolution. The Cl 3p nonbonding orbitals have much broader spatial distributions than the F 2p nonbonding orbitals, and thus the orbitals possess sharply peaked momentum distributions, which may have suffered from the influence of the momentum resolution employed. The fitting analysis indicates that although their accuracies depend on the instrumental momentum resolution, internuclear distances can be derived from bond oscillation.

To get further insights into the interference phenomena, we subsequently discuss distorted-wave effects on bond oscillation in more detail. As was mentioned, the effects on the momentum profiles of CCl_4 are substantial at $p >\sim 1.6$ a.u., and hence the following discussion is mainly focused on the high p region. In the present bond oscillation analysis, the influence of distorted-wave effects was taken into account only through the DWBA Cl 3p cross section, $\sigma_{3p}(p)$, by assuming that the effects do not cause to any change in the interference factor, $I_\alpha(p)$. In spite of this approximation used, the analytic interference factor (chain line) has qualitatively accounted for the observed oscillatory structures for CCl_4 and CF_4. It appears to support the assumption for $I_\alpha(p)$.

Nevertheless, for CCl_4, a close look at Figure 3a shows that the agreement between experiment and the fitting curve is not quantitative; the experiment exhibits smaller oscillation amplitude and higher intensity than the analytic interference factor at $p >\sim 1.6$ a.u., where substantial distorted-wave effects have been observed in the $(2t_1{+}7t_2 + 2e)$ momentum profile. On the other hand, for CF_4, the experimental interference pattern has been well reproduced by the fitting curve even at large p. Here we point out that the distorted-wave effects on large p components are more pronounced for the molecules containing heavier atoms due to their higher nuclear charges [27]. Indeed, the difference of the experimental momentum profile from the PWIA prediction is much larger for CCl_4 than CF_4 at $p > 1.6$ a.u. For instance, the $(2t_1{+}7t_2 + 2e)$ experimental momentum profile of CCl_4 exhibits as much as a factor of $\sim$4 higher intensity than the PWIA calculation at $p = 2.4$ a.u., while the intensity difference between experiment and theory is only 3% for the $(1t_1{+}4t_2 + 1e)$ momentum profile of CF_4. It would therefore be reasonable to think that for CCl_4, not only $\sigma_{3p}(p)$ but also $I_\alpha(p)$ is appreciably influenced by the significant distorted-wave effects at large p.

Here it is worthwhile to note that the oscillation observed in the momentum profiles can also be recognized as a result of four-center interference effects in EMS cross sections, i.e., coherent (e, 2e) scattering from the four different atomic centers. In this regard, bond oscillation may be a phenomenon analogous to the Cohen-Fano oscillations [39] or the Young-type double-slit interference [40,41]. Thus, the bond oscillation provides an opportunity to examine the influence of distortion of the electronic waves caused by the target potential to the Young-type double-slit interference. For CCl_4, the smaller oscillation amplitude compared to the fitting curve observed at $p >\sim 1.6$ a.u. strongly suggests that distorted-wave effects lead to the partial destruction of the interference of the scattering amplitudes.

5 Conclusion

In this study we have carried out the EMS experiment for the three outermost orbitals of CCl_4, which are each constructed from the Cl 3p AOs, as well as the $6t_2$ and $6a_1$ orbitals. The comparison of the experiment with the associated PWIA calculation has shown that distorted-wave effects are substantial for the momentum profiles of these MOs at $p >\sim 1.6$ a.u. The interference pattern of the Cl 3p nonbonding orbitals has then been obtained by dividing the $(2t_1{+}7t_2 + 2e)$ experimental momentum profile by the DWBA cross section of the Cl 3p AO, and it has been compared with that for the F 2p nonbonding orbitals of CF_4. The comparison for these molecules has clearly shown that the period of interference pattern reflects the molecular structure, and a fitting analysis has demonstrated that internuclear distances can be extracted from bond oscillation. Furthermore, the distortion of the incoming and outgoing electron waves has been found to considerably affect the interference pattern for CCl_4 at large momentum. The present result strongly suggests that the distorted-wave effects partially destruct the interference of scattering amplitudes for (e, 2e) electron impact ionization from the four different Cl atomic centers. Since EMS allows one to examine the interference phenomena from small p, at which the PWIA provides a good description, to large p, where distorted-wave effects are substantial, it can provide an opportunity to comprehensively investigate how distortion of the electron waves from plane-waves affect the Young-type double-slit interference.

This research was supported by the Ministry of Education, Culture, Sports, Science and Technology, Grant-in-Aids for Scientific Research (A) (No. 25248002), (B) (No. 15H03761), and Grant-in-Aid for Challenging Exploratory Research (Nos. 25620006 and 15K13615).

References

1. I.E. McCarthy, E. Weigold, Phys. Rep. **27**, 275 (1976)
2. C.E. Brion, Int. J. Quantum Chem. **29**, 1397 (1986)
3. K.T. Leung, in *Theoretical Models of Chemical Bonding*, Part 3, edited by Z.B. Maksic (Springer-Verlag, Berlin, 1991), pp. 339–386
4. I.E. McCarthy, E. Weigold, Rep. Prog. Phys. **54**, 789 (1991)
5. M.A. Coplan, J.H. Moore, J.P. Doering, Rev. Mod. Phys. **66**, 985 (1994)
6. E. Weigold, I.E. McCarthy, *Electron Momentum Spectroscopy* (Kluwer Academic/Plenum Publishers, New York, 1999)
7. M. Takahashi, Bull. Chem. Soc. Jpn **82**, 751 (2009)
8. C.A. Coulson, Proc. Cambridge Philos. Soc. **37**, 55 (1941)
9. C.A. Coulson, W.E. Duncanson, Proc. Cambridge Philos. Soc. **37**, 67 (1941)
10. I.R. Epstein, A.C. Tanner, in *Compton Scattering*, edited by B.G. Williams (McGraw-Hill, New York, 1977)
11. J.P.D. Cook, C.E. Brion, Chem. Phys. **69**, 339 (1982)
12. N. Watanabe, X.-J. Chen, M. Takahashi, Phys. Rev. Lett. **108**, 173201 (2012)
13. Z. Zhang, X. Shan, T. Wang, E. Wang, X. Chen, Phys. Rev. Lett. **112**, 023204 (2014)
14. M. Yamazaki, H. Satoh, N. Watanabe, D.B. Jones, M. Takahashi, Phys. Rev. A **90**, 052711 (2014)
15. M. Zhao, X. Shan, J. Yang, E. Wang, S. Niu, X.-J. Chen, Chin. J. Chem. Phys. **28**, 539 (2015)
16. N. Watanabe, M. Yamazaki, M. Takahashi, J. Electron Spectrosc. Relat. Phen. **209**, 78 (2016)
17. M. Takahashi, N. Watanabe, Y. Khajuria, K. Nakayama, Y. Udagawa, J.H.D. Eland, J. Electron Spectrosc. Relat. Phenom. **141**, 83 (2004)
18. A.M. Grisogono, R. Pascual, W. Von Nissen, E. Weigold, Chem. Phys. **135**, 317 (1989)
19. P. Duffy, D.P. Chong, M.E. Casida, D.R. Salahub, Phys. Rev. A **50**, 4707 (1994)
20. A.D. Becke, J. Chem. Phys. **98**, 5648 (1993)
21. T.H. Dunning Jr., J. Chem. Phys. **90**, 1007 (1989)
22. M.J. Frisch et al., *Gaussian 03 Revision A.1* (Gaussian Inc., Pittsburgh, PA, 2003)
23. A.O. Bawagan, C.E. Brion, E.R. Davidson, D. Feller, Chem. Phys. **113**, 19 (1987)
24. J.N. Migdall, M.A. Coplan, D.S. Hench, J.H. Moore, J.A. Tossell, V.H. Smith Jr., J.W. Liu, Chem. Phys. **57**, 141 (1981)
25. W. von Niessen, L. Åsbrink, G. Bieri, J. Electron Spectrosc. Relat. Phenom. **26**, 173 (1982)
26. K. Kimura, S. Katsumata, Y. Achiba, T. Yamazaki, S. Iwata, *Handbook of He I Photoelectron Spectra of Fundamental Organic Molecules* (Japan Scientific Society, Tokyo, 1981)
27. Y. Miyake, M. Takahashi, N. Watanabe, Y. Khajuri, Y. Udagawa, Y. Sakai, T. Mukoyama, Phys. Chem. Chem. Phys. **8**, 3022 (2006)
28. N. Watanabe, Y. Khajuri, M. Takahashi, Y. Udagawa, J. Electron Spectrosc. Relat. Phenom. **142**, 325 (2005)
29. N. Watanabe, M. Yamazaki, M. Takahashi, J. Chem. Phys. **137**, 114301 (2012)
30. B. Hajgatoì, F. Morini, M.S. Deleuze, Theor. Chem. Acc. **131**, 1244 (2012)
31. N. Watanabe, M. Yamazaki, M. Takahashi, J. Chem. Phys. **141**, 244314 (2014)
32. J. Yang, X. Shan, Z. Zhang, Y. Tang, M. Zhao, X.-J. Chen, J. Phys. Chem. A **118**, 11780 (2014)
33. F. Morini, M.S. Deleuze, N. Watanabe, M. Takahashi, J. Chem. Phys. **142**, 094308 (2015)
34. F. Morini, N. Watanabe, M. Kojima, M.S. Deleuze, M. Takahashi, J. Chem. Phys. **143**, 134309 (2015)
35. I.E. McCarthy, Aust. J. Phys. **48**, 1 (1995)
36. E. Clementi, C. Roetti, At. Data Nucl. Data Tables **14**, 177 (1974)
37. L.S. Bartell, L.O. Brockway, R.H. Schwendeman, J. Chem. Phys. **23**, 1854 (1955)
38. M. Fink, C.W. Schmiedekamp, D. Gregory, J. Chem. Phys. **71**, 5238 (1979)
39. H.D. Cohen, U. Fano, Phys. Rev. **150**, 30 (1966)
40. M.F. Ciappina, O.A. Fojón, R.D. Rivarola, J. Phys. B **47**, 042001 (2014)
41. D. Akoury, K. Kreidi, T. Jahnke, Th. Weber, A. Staudte, M. Schöffler, N. Neumann, J. Titze, L.Ph.H. Schmidt, A. Czasch, O. Jagutzki, R.A. Costa Fraga, R.E. Grisenti, R. Díez Muiño, N.A. Cherepkov, S.K. Semenov, P. Ranitovic, C.L. Cocke, T. Osipov, H. Adaniya, J.C. Thompson, M.H. Prior, A. Belkacem, A.L. Landers, H. Schmidt-Böcking, R. Dörner, Science **318**, 949 (2007)